nature communications

Article

https://doi.org/10.1038/s41467-024-54092-6

Earth's longest preserved linear volcanic ridge generated by a moving Kerguelen hotspot

Received: 14 February 2024

Accepted: 1 November 2024

Published online: 08 November 2024

Check for updates

Qiang Jiang[1,2,3] ✉, Hugo K. H. Olierook[4], Fred Jourdan[3], Diana Carmona Hoyos[3], Renaud E. Merle[5], Evelyn M. Mervine[6] & William W. Sager[7]

Recent seismic tomography unveiled complex mantle plume structures diverging from the originally proposed single, narrow, and vertically-oriented plume conduits, which necessitates new perspectives on the mechanism of hotspot motion. While several recent endeavours have focused on Pacific hotspots' motion, knowledge of others remains limited. Here we constrain the motions of the Kerguelen hotspot within the Indian Ocean by obtaining robust $^{40}Ar/^{39}Ar$ ages for the Ninetyeast Ridge, Earth's longest linear volcanic ridge. These data indicate varying volcanic progression rates along the ridge, contrasting to a constant rate as previously documented. Combined with constraints on the Indian Plate motion and seafloor spreading, we reveal four periods of motions of the hotspot caused by its interactions with the Indian–Antarctic spreading ridge. This suggests that mantle plume lateral flows are susceptible to changes in shallow mantle convection due to the existence of horizontal ponding zones and vertical conduits, especially in the shallow asthenosphere.

Hotspots are unique features on Earth's surface that act as a window to probe the deep mantle and mantle convection processes through the underlying mantle plumes that feed them, and as a reference frame to track the absolute motion of tectonic plates. Originally, it was proposed that hotspots were stationary[1]. Subsequent palaeomagnetism, geochronology, and geodynamics research indicated that hotspots are not fixed and that the magnitude of hotspot motions could be as significant as plate motions[2–5]. Still uncertain is the cause of hotspot mobility, which hampers our ability to constrain the past location of hotspots and thus affects the reliability of absolute reference frames based on moving hotspots. It is unclear whether shallow or deep mantle processes are the dominant controlling factor on hotspot motion[6]. Examples of the former include tectonic plate-driven horizontal mantle shear[7–9] and the effect of spreading ridges[10,11]. Conversely, large-scale mantle winds[10], or the motions of zones of the deepest mantle where mantle plumes were believed to be rooted (e.g., large low shear velocity provinces, or LLSVPs), have also been attributed to be the cause of hotspot motions[12–14].

Many of the explanations of hotspot motions were built upon the classic model that hotspots are manifestations of narrow, vertical, pipe-like mantle plume upwellings from the lower mantle[1,10,14]. However, based on improved seismic tomographic techniques and due to the increasing availability of seismic data, more complex mantle plume structures have been imaged[15–17]. Some of these tomographic models show that at the core-mantle boundary, LLSVPs extend as a wide continuous trunk to ~1500-km depth, which then branches into

[1]State Key Laboratory of Petroleum Resources and Engineering, China University of Petroleum, Beijing, China. [2]College of Geosciences, China University of Petroleum, Beijing, China. [3]Western Australian Argon Isotope Facility, John de Laeter Centre, School of Earth and Planetary Sciences, Curtin University, Perth, WA, Australia. [4]Timescales of Mineral Systems Group, School of Earth and Planetary Sciences, Curtin University, Perth, WA, Australia. [5]Department of Earth Sciences, Natural Resources and Sustainable Development, Uppsala University, Uppsala, Sweden. [6]School of the Environment, The University of Queensland, St. Lucia, QLD, Australia. [7]Department of Earth and Atmospheric Sciences, University of Houston, Houston, TX, USA. ✉e-mail: q.jiang@cup.edu.cn

complex shapes upward towards hotspots[15,18]. Most recently, based on full waveform shear wave tomography, Dongmo Wamba et al.[16] revealed a bundle of 'fat' mantle plumes rising quasi-vertically from LLSVPs. Each of these mantle plumes spreads laterally after rising to a depth of 1000 and 660 km and forms a ponding zone, from which a thinner plume rises quasi-vertically to a depth of 250–100 km and forms a shallower level of horizontal ponding zone, which then feeds magma to the surface to form a hotspot. These newly discovered mantle plume structures necessitate new interpretations of why and how hotspots moved in response to mantle plumes' interactions with shallow and deep mantle processes.

The majority of previous efforts in the past decade to constrain the motions of hotspots are focused on the Pacific hotspots, particularly the Hawaii hotspot that created the iconic Hawaiian-Emperor bend[6,11,13,14,19] and the Louisville and Rurutu hotspots[3,20], but relatively limited attention has been given to other hotspots, including those in the Indian Ocean. The Kerguelen hotspot, which is currently located at the Kerguelen Archipelago[21] or Heard Island and McDonald Islands[22,23] where there has been recent volcanism, is fed by the Kerguelen mantle plume that formed the Cretaceous Kerguelen large igneous province[24–26], and the north–south-oriented Ninetyeast Ridge[27,28], which spans over 5000 km and is the longest preserved volcanic lineament on Earth (Fig. 1). Previous work has tested whether the Kerguelen hotspot has remained fixed and, if not, how and why it moved during the formation of the Kerguelen large igneous province and the Ninetyeast Ridge[29–35]. Early paleomagnetic data of basalts from ocean drilling holes on the Kerguelen Plateau and the Ninetyeast Ridge, combined with tectonic and geochronological constraints of the basaltic basement, indicate that the Kerguelen hotspot may have moved southwards[34,35] (Supplementary Information) or westwards[29], but these results are far from conclusive due to either insufficient drilling depth of the basaltic basement to average out geomagnetic paleosecular variation (e.g., Sites 254, 748, and 1140)[34–36] or post-magmatic magnetic overprints (e.g., Sites 1140 and 758[34,35]; cf. detailed discussions in Supplementary Information; Fig. S1). Depending on different assumptions about the source of the hotspot and the choice of parameters, numerical modelling has shown various motion histories for the Kerguelen hotspot. For example, some researchers suggested that the Kerguelen hotspot may have moved in a south-easterly direction[30–32], while Steinberger et al.[33] proposed that the Kerguelen hotspot may have moved towards the northwest or have little overall motion in the past 100 Myr.

The propagation rate of volcanoes along a hotspot track, when combined with knowledge about the rate of plate motions, can also illustrate the absolute motion of a hotspot[37–39]. Quantifying the progression rate requires robust and precise radioisotopic ages of basalts from the hotspot track. As a track of the Kerguelen hotspot, the Ninetyeast Ridge lacks reliable and high-precision geochronology data. Although radioisotopic age determinations were published[27,40] for volcanic basement rocks that had been collected during three ocean drilling expeditions, a critical evaluation of these ages revealed that they were not statistically reliable (Table S1, Supplementary Information). Moreover, these ages were all obtained from groundmass, which is susceptible to seawater alteration in contrast to data generated from plagioclase separates according to recent studies[41–43] and data in this study (Supplementary Information). Additional $^{40}Ar/^{39}Ar$ dating results of basalts dredged during an R/V *Roger Revelle* expedition were presented in conference abstracts[44–46], but these results were never published, and neither the analytical procedures nor analytical data are available to allow reliability assessment of the ages, which therefore cannot be used to constrain the age progression rate of the Ninetyeast Ridge.

Here, we present robust and precise $^{40}Ar/^{39}Ar$ ages for basalt samples from the Ninetyeast Ridge to study the rate of volcanic progression along the ridge. Combined with constraints on the migrations of the Indian Plate and seafloor spreading, we investigate the motion history of the Kerguelen hotspot during the formation of the Ninetyeast Ridge, explore the potential causes, and discuss its implications for the mechanisms of hotspot motion in the context of an improved understanding of the structure of mantle plumes.

Results and discussion

$^{40}Ar/^{39}Ar$ ages for the Ninetyeast Ridge

We conducted $^{40}Ar/^{39}Ar$ geochronology analyses on basalt samples collected from cores recovered by Deep Sea Drilling Project (DSDP) Legs 22 and 26 and Ocean Drilling Program (ODP) Leg 121 as well as dredge samples from R/V *Roger Revelle* expedition KNOX06RR to the Ninetyeast Ridge (Figs. S2–S4, Supplementary Information). A total of 13 robust plagioclase $^{40}Ar/^{39}Ar$ plateau ages revealed an overall age progression from north to south along the ridge (Fig. 1, Figs. S5–S15, Table S2; cf. robustness criteria in Supplementary Information). The northernmost Site 758 yielded the oldest age of 83.0 ± 2.5 Ma (Fig. S5). Site 216, which is ~440 km south of Site 758, yielded an age of 71.6 ± 1.2 Ma (Fig. S6). Samples from Dredge Site #6 yielded two precise ages of 65.85 ± 0.13 Ma and 66.36 ± 0.53 Ma, which resulted in a weighted mean age of 65.88 ± 0.13 Ma (Fig. S8). On the central segment of the Ninetyeast ridge, Site 214 yielded a $^{40}Ar/^{39}Ar$ plateau age of 62.41 ± 0.52 Ma (Fig. S9), and Site 757 yielded an average age of 52.5 ± 1.0 Ma (Fig. S10). On the south segment, two dredge samples, which are ~400 km apart, yielded $^{40}Ar/^{39}Ar$ plateau ages of 49.13 ± 0.32 Ma (Dredge Site #30; Fig. S11) and 45.90 ± 0.30 Ma (Dredge Site #33; Fig. S12), respectively.

The robust plagioclase separates $^{40}Ar/^{39}Ar$ ages for the Ninetyeast Ridge suggest that the ages of volcanism along the Ninetyeast Ridge did not progress northwards at a constant rate of 94 km Myr^{-1} or 118 km Myr^{-1} as previously inferred from unreliable groundmass $^{40}Ar/^{39}Ar$ ages (Table S1)[27,40] and undocumented $^{40}Ar/^{39}Ar$ dating results (cf. discussions in Supplementary Information)[28,45,46], but instead displays changing age progression along the ridge (Fig. 2). Specifically, the age of the Ninetyeast Ridge progressed northwards during four stages with different average rates along the ridge: (I) 47 mm yr^{-1} from 83 Ma to 66 Ma, (II) 302 mm yr^{-1} from 66 Ma to 62 Ma, (III) 64 mm yr^{-1} from 62 Ma to 53 Ma, and (IV) 147 mm yr^{-1} from 53 Ma to 46 Ma (Fig. 2B).

Motion of the Kerguelen hotspot

The Ninetyeast Ridge was formed by the Kerguelen mantle plume during the opening of the Indian Ocean when the Indian Plate was drifting northwards[47], before Greater India collided with the Eurasian Plate[48] (Fig. S16). If the Kerguelen hotspot remained fixed underneath the Indian Plate during the formation of the Ninetyeast Ridge, the volcanic progression rate of the Ninetyeast Ridge would be the same as the rate of northward movement of the Indian Plate. Given that the Eurasian Plate remained near-stationary during the considered period of time[49,50], the Indian Plate's northward migration rate would be nearly identical to the rate of convergence between India and Eurasia (Fig. 2D). Since the Antarctic and Eurasian Plates remained relatively stationary[49,50], the migration rate of the Indian Plate would also be nearly equal to the rate of oceanic crust creation (hence the rate of seafloor spreading; Fig. 2C) between the Antarctic and Indian Plates, which filled the space between the two plates. Therefore, under the assumption of a fixed Kerguelen hotspot underneath the Indian Plate, the rate of volcanic progression of the Ninetyeast Ridge would be nearly identical to the rate of seafloor spreading between the Antarctic and Indian Plates, and the rate of convergence between India and Eurasia. Considering that the rate of seafloor spreading and the India–Eurasia convergence rate show similar values[51] (Fig. 2), we focus our discussions on the former in this study hereafter. By comparing the progression rate of the Ninetyeast Ridge volcanism and the spreading rate of the Indian–Antarctic spreading ridge (Fig. 2), we can examine

https://doi.org/10.1038/s41467-024-54092-6

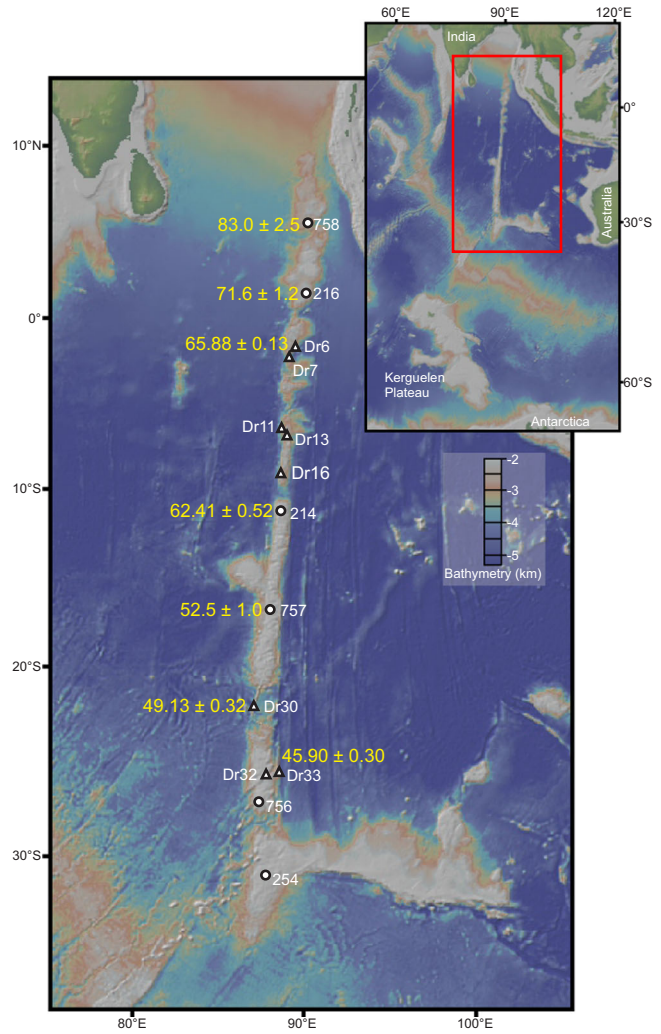

Fig. 1 | Bathymetric map of the Ninetyeast Ridge, annotated with $^{40}Ar/^{39}Ar$ ages. The ages (yellow text) are in Ma with 2σ uncertainty. DSDP and ODP drill sites and dredge sites (white text) that were dated are shown as solid white circles and triangles, respectively. Inset shows the location of the Ninetyeast Ridge in the Eastern Indian Ocean. The bathymetric map was generated using GeoMapApp[73] (www.geomapapp.org), https://creativecommons.org/licenses/by/4.0/.

the mobility of the Kerguelen hotspot during the formation of the Ninetyeast Ridge.

During Stage I (~83–66 Ma), the age progression rate (~47 mm yr^{-1}) is roughly half of the spreading rate (Fig. 2), meaning that the Kerguelen hotspot was not fixed beneath the Indian Plate. At this stage, the most likely scenario is that the mantle plume was captured by the northward-migrating Indian–Antarctic spreading ridge, and plume materials flowed continuously towards the spreading ridge and erupted at the ridge (Fig. 3A; Fig. S17A). Considering that the Kerguelen mantle plume was located in a region of overall north- to north-eastward uppermost mantle flow since it rises from the southeastern corner of the African large low shear velocity province (LLSVP)[52], the plume conduit may have been located south of the spreading ridge and plume–ridge interaction occurred in the form of northward plume flow (plume conduit tilting) towards the spreading ridge (Fig. S17A).

Although the volcanic progression rate of the Ninetyeast Ridge can also result from a northward moving hotspot beneath the Indian Plate, or a southward moving hotspot beneath the Antarctic Plate, both at a rate of ~47 mm yr^{-1} (Fig. S17), it is hard to explain why the hotspot moved at a rate that is approximately the half spreading rate in both scenarios. In contrast, for a stationary Antarctic Plate, the spreading ridge would move at half the spreading rate, so the age progression is nicely consistent with the eruption of plume material at the spreading ridge. The proximity and interactions between the spreading ridge and the Kerguelen mantle plume are supported by the geochemical and isotopic studies of basalts from the Ninetyeast Ridge (Fig. S18, Supplementary Data 2)[53–56], which revealed both a depleted mantle source component similar to that of mid-ocean ridge basalt compositions and an enriched mantle plume component as represented by the compositions of isotopically radiogenic mildly alkali basalts from the Kerguelen Archipelago[57,58].

During Stage II (~66–62 Ma), the 302 mm yr^{-1} age progression rate is nearly two times the full-spreading rate (Fig. 2). At this stage, the Ninetyeast Ridge crossed the 89°E fracture zone and began to form on the west side of the fracture zone (Fig. S19), and the segment of the Indian–Antarctic spreading ridge jumped southwards slightly (~200 km) at ~65 Ma[28]. Following these events and considering the changes in the volcanic progression rate of the Ninetyeast Ridge, a possible scenario is that the spreading ridge segment that captured the Kerguelen mantle plume at Stage I had migrated too far northward to sustain its interaction with the mantle plume, thus the mantle plume disconnected from it and moved southwards towards the spreading ridge segment west of the 89°E fracture zone at a rate of ~150 mm yr^{-1} (i.e., age progression rate minus spreading rate). The various degrees of involvement of depleted components in the mantle source of the Ninetyeast Ridge as indicated by geochemical data[53–56] (Fig. S18) may result from the changing distance between the Kerguelen mantle plume and spreading ridge segments during this stage.

Nevertheless, given that there are currently only two age data (i.e., 65.88 ± 0.13 Ma for Dredge Site #6 and 62.41 ± 0.52 Ma for DSDP Site 214) available to define the age progression rate along the Ninetyeast Ridge for this stage, the motion of the Kerguelen hotspot and the seemingly high migration rate (~150 mm yr^{-1}) still needs to be better constrained. Moreover, although the $^{40}Ar/^{39}Ar$ spectra for Dredge Site #6 (Fig. S7, Table S2) meet all our strict criteria for a robust $^{40}Ar/^{39}Ar$ age (Supplementary Information), the Ca/K spectra show a slightly tilde-shaped pattern (Fig. S7), which indicates there is the possibility that the plagioclase samples may have been affected by alteration[41]. In such a possible scenario, the modelling results of Jiang et al.[41] showed that the sample's real age might be slightly (e.g., ~3%), but not considerably, older than the measured age given the statistically robust $^{40}Ar/^{39}Ar$ age spectra. As a result, the age progression rate at Stage II could be ~190 mm yr^{-1}, which is slightly greater than the spreading rate (~155–180 mm yr^{-1}; Fig. 2B), meaning that the hotspot motion rate would be ~10–35 mm yr^{-1} at this stage.

During Stage III (~62–53 Ma), the age progression decreased significantly to ~64 mm yr^{-1} (Fig. 2B), nearly half of the spreading rate, which decreased to ~130 mm yr^{-1} (Fig. 2C). This indicates that the Kerguelen mantle plume was connected to the spreading ridge segment west of the 89°E fracture zone and plume materials flowed northward and erupted again at the spreading ridge (Fig. 3C).

For Stage IV (~53–46 Ma), the spreading rate gradually decreased from ~120 mm yr^{-1} to ~70 mm yr^{-1}, while the age progression rate of the Ninetyeast Ridge increased to 147 mm yr^{-1} (Fig. 2), suggesting that the mantle plume disconnected from the spreading ridge segment immediately west of the 89°E fracture zone and moved southwards towards the next spreading ridge segment (Fig. 3). Given that there was no indication that the Ninetyeast Ridge crossed another fracture zone at this stage (Fig. S19), the hotspot remained at the south side of the spreading ridge and thus the migration rate was 147 mm yr^{-1}.

After Stage IV, a large ridge jump at ~42 Ma[28] and spreading ridge re-organizations[47] (Fig. S16) may have transferred the Ninetyeast Ridge segment formed on the Antarctic Plate to the Indian Plate. Since our geochronology analyses for samples formed in this period (Sites 756 and 254; Table S2) did not yield robust and precise age data, the detailed history of the formation of these Ninetyeast Ridge segments

https://doi.org/10.1038/s41467-024-54092-6

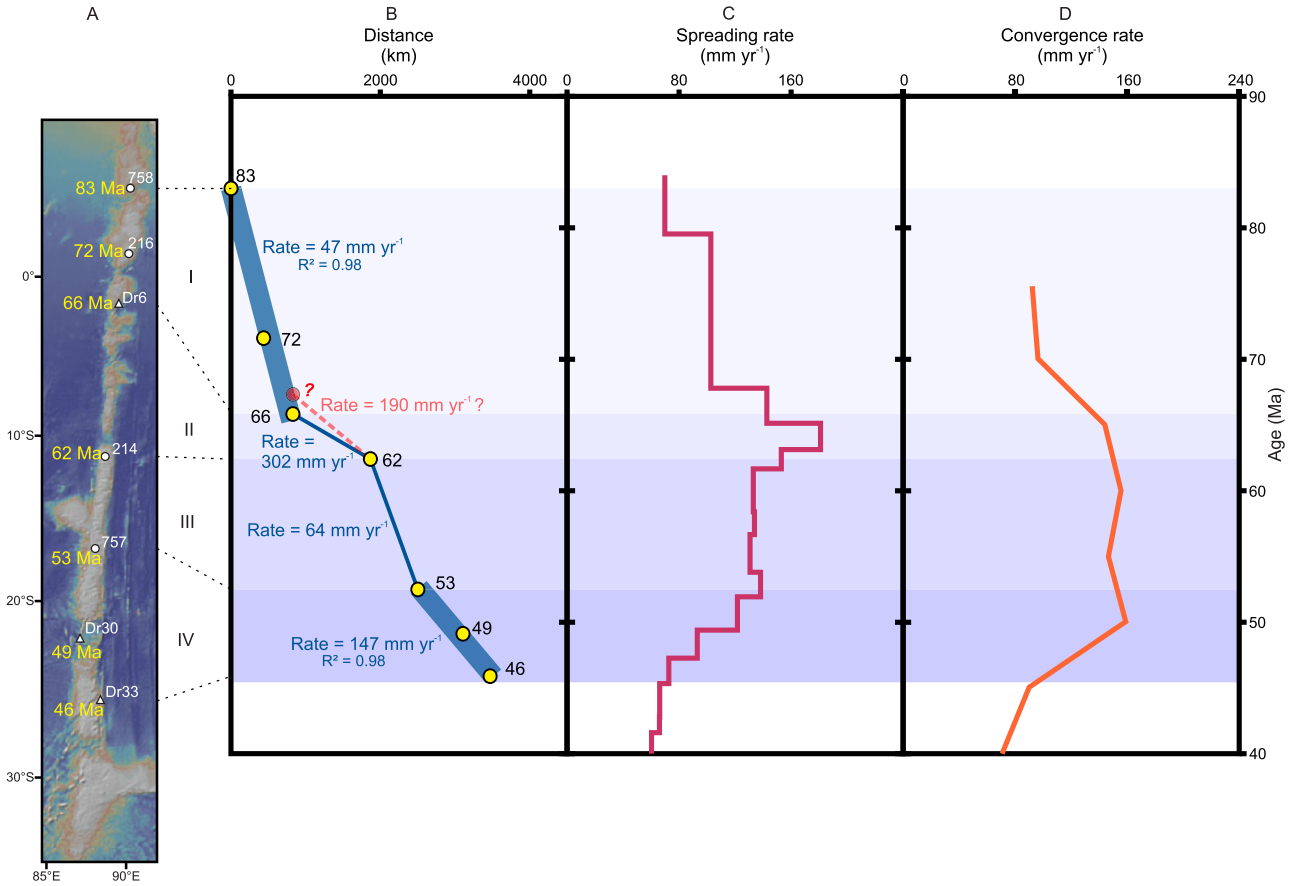

Fig. 2 | Temporal variations of rates of age progression along the Ninetyeast Ridge, the Indian–Antarctic spreading, and the India–Eurasia convergence. **A** Bathymetric map of the Ninetyeast Ridge. The bathymetric map was generated using GeoMapApp[73] (www.geomapapp.org), https://creativecommons.org/licenses/by/4.0/. **B** Temporal variation of progression rates of volcanism along the Ninetyeast Ridge. **C** Spreading rate of the Indian–Antarctic spreading ridge vs time based on magnetic anomaly and fracture zone data[49,74]. **D** Convergence rate between India and Eurasia vs time[75].

and the motions of the Kerguelen hotspot after ~46 Ma remains to be further explored in future studies. After the formation of the entire Ninetyeast Ridge, the Kerguelen hotspot was located beneath the fixed Antarctic Plate and formed the Northern Kerguelen Plateau and portions of the Central Kerguelen Plateau[22,59–61].

In summary, our data show that the Kerguelen mantle plume was captured by two segments, separated by the 89°E fracture zone, of the Indian–Antarctic spreading ridge at ~83–66 Ma, and ~62–53 Ma, respectively, and migrated northwards together with the spreading ridge. During ~66–62 Ma and ~53–46 Ma, the mantle plume disconnected from the previous spreading ridge segment and moved southwards towards another spreading ridge segment (Fig. 3). Given that robust age data for the Ninetyeast Ridge are currently still limited, particularly for Stages II and III where the age progression rates were all calculated using two age data points per stage on the ridge segment (Fig. 2B), constraints on when exactly the volcanic progression rate changed and how long each stage lasted remain to be improved by further sampling and analyses.

Mechanisms of hotspot motion

The motions of the Kerguelen hotspot during the formation of the Ninetyeast Ridge were most likely controlled by the influence of the Antarctic–Indian spreading ridge based on the above discussions. This influence includes (i) directly trapping of the mantle plume by the spreading ridge segments, which occurred in the form of lateral plume flow in the shallow mantle and plume conduit tilting towards a spreading ridge (Fig. 3A, C); (ii) disconnecting process of the mantle plume from the spreading ridge, likely resulting from the increased distance between the spreading ridge and the plume conduit, during which the mantle plume moved away from the spreading ridge, and (iii) re-capturing process of the mantle plume by another spreading ridge segment, during which time the hotspot migrated southwards (Fig. 3B, D). The multiple stages of plume–ridge interactions during the formation of the Ninetyeast Ridge were enabled by the continuous northward migration of the Indian–Antarctic spreading ridge, and the segmentation of the spreading ridge by large transform faults (Figs. 3, S19).

Although deeper mantle convection has also been proposed to be the trigger of hotspot motions in the Pacific Ocean[6,10,14], this mechanism seems unlikely to be the driver of the Kerguelen hotspot motions. Specifically, the hypothesis that the deformation and motion of the lowermost mantle on which hotspots are anchored (e.g., due to the descent of subducted slabs) triggered hotspot motion[12–14] cannot satisfactorily explain the Kerguelen hotspot motions. Such motions of the lowermost mantle were usually associated with long-lasting ancient subduction events[14], which seems implausible to have controlled the quickly changing directions and rates for the Kerguelen hotspot motions over a few tens of million years (Figs. 2, 3).

The motion history of the Kerguelen hotspot during the formation of the Ninetyeast Ridge revealed in this study indicates that it was different from that of other Indian Ocean hotspots. For example, the Reunion hotspot moved northwards by ~5° between ~55 Ma and 35 Ma[32,62], while the Marion hotspot may have stayed stationary according to paleomagnetic data[63] or moved ~7° southwards based on numerical modelling results[7,32] in the past ~90 Ma. These indicate that

https://doi.org/10.1038/s41467-024-54092-6

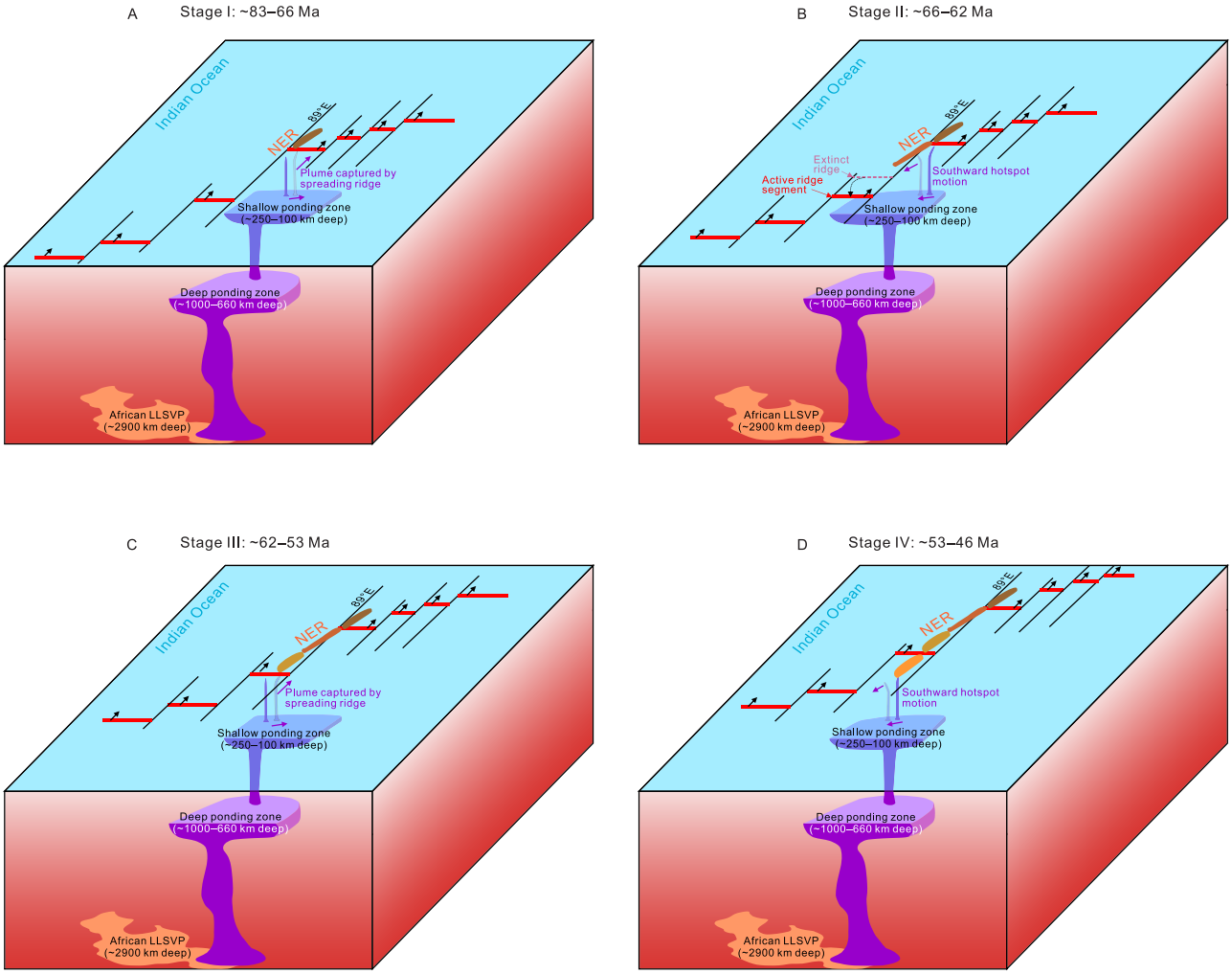

Fig. 3 | Schematic diagrams showing the formation of the Ninetyeast Ridge and the motions of the Kerguelen hotspot. A Stage I from ~83 Ma to 66 Ma. **B** Stage II from ~66 Ma to 62 Ma. **C** Stage III from ~62 Ma to 53 Ma. **D** Stage IV from ~53 Ma to 46 Ma. The structure of the mantle plume refers to Dongmo Wamba et al.[16]. The scale of the plume structure above the mantle ponding zones in the upper mantle is exaggerated in order to demonstrate its interaction with the spreading ridges. The red and black lines indicate the Indian–Antarctic spreading ridges and fracture zones, respectively. The red dashed line indicates an extinct spreading ridge segment. The black and purple arrows indicate the motions of the Indian–Antarctic spreading ridges and the Kerguelen hotspot, respectively. The Kerguelen mantle plume rises from the southeastern corner of the African large low shear velocity province (relative size exaggerated for the plume)[52]. NER Ninetyeast Ridge, LLSVP large low shear velocity province.

the Indian Ocean hotspots moved independently, in a similar fashion as that of the Pacific hotspots[3,20]. Like that of the Pacific Ocean hotspots[3], the motions of the Indian Ocean hotspots are also controlled by regional mantle flows rather than by a hypothesised large-scale mantle convection[2,10].

Our results thus stress the important role of upper mantle convection on the motion of a hotspot. The fact that hotspots on the Earth's surface may have been directly fed by a ponding zone in the asthenosphere at depths of ~250 to 100 km (Fig. 3)[16] implies that hotspot motions, at least for those that share similar geodynamic settings as the Kerguelen hotspot, may be more responsive to mantle upwelling at spreading ridges in the shallow mantle than motions in the deep mantle. For disturbances in the deep mantle (e.g., the arrival of subducted slabs at the LLSVPs)[14], if they indeed can trigger the motion of a hotspot on the surface in a 'bottom-up' manner[6,12,14], these perturbations on the mantle plume in the deep mantle would have to pass through one or more plume material ponding zones in the shallower mantle[16]. These plume ponding zones may not be as responsive to disturbances on a mantle plume compared with the scenario of a single, narrow plume conduit.

Implications for lateral mantle plume flow

Recent seismic tomography studies have revealed large lateral mantle plume flows towards spreading ridges, for example, from the vertical plume conduit underneath eastern Greenland towards Iceland (~800 km)[64], and from the Réunion hotspot to the Central Indian Ridge (~1200 km)[65]. These geophysical observations, however, provided only a snapshot of the current state of the mantle, while the processes of how mantle plumes and spreading ridges were coupled and disconnected remain unclear. Our data imply that the Kerguelen hotspot experienced ~800 km and ~576 km northward movements when the mantle plume was trapped by segments of the northward migrating Indian–Antarctic spreading ridge at ~83–66 Ma and ~62–53 Ma, respectively. These magnitudes of lateral plume flow are possible when considering the examples of the Iceland and Réunion mantle plumes[64,65], and could be achieved by both tilting of the plume conduit and drifting of the plume material in the shallower ponding zone in the shallow mantle (Fig. 3).

When the plume began to disconnect from the previous spreading ridge segment that it was connected to, and move towards the next spreading ridge segment during ~66–62 Ma and ~53–46 Ma,

respectively, the hotspot moved at very high rates (~150 mm yr^{-1} and 147 mm yr^{-1}, respectively). These rates are significantly higher than the average moving rates of hotspots elsewhere, for example, the ~40–50 mm yr^{-1} for the motions of the Hawaii hotspot during 80–50 Ma[2,13]. This indicates that the capturing and releasing of a mantle plume by a spreading ridge was a rapid process that happened in a short duration of a few million years.

The frequently and quickly changing directions and rates of the Kerguelen hotspot during Ninetyeast Ridge's formation might be a reflection of changes in the lateral plume flow. The existence of both quasi-vertical conduits and horizontal ponding zones, particularly in the shallow asthenospheric mantle, makes the lateral flows of mantle plumes susceptible to changes in shallow mantle convection processes such as the presence and drifting apart of spreading ridges.

Methods

Details regarding $^{40}Ar/^{39}Ar$ analytical results, literature paleomagnetic paleolatitudes, evaluation of literature geochronology data, and literature plate reconstruction and geochemical results for the Ninetyeast Ridge are provided in the Supplementary Information.

Sample description

Volcanic basement rocks have been collected during the DSDP Legs 22 and 26 drilling expeditions in 1972, the ODP Leg 121 drilling expedition in 1988, and an R/V *Roger Revelle* expedition (KNOX06RR) in 2007. Based on the availability of volcanic rocks that appear to be fresh, we requested 32 basaltic samples from DSDP Sites 214, 216, and 254, and ODP Sites 756, 757, and 758 (Figs. S2–S3) from the Kochi Core Center (Japan); and 17 samples from 6 dredge sites of the R/V *Roger Revelle* expedition from the Woods Hole Oceanographic Institution Seafloor Samples Repository (USA). Most of the dredge samples are pillow lavas, and are generally more altered than the DSDP and ODP drilling samples. Regardless, many lightly altered, plagioclase-rich rocks are recovered from the dredges.

Thin sections were made for 43 samples that appear to be fresh. Through careful thin section examinations, we selected 22 volcanic rocks that contain a substantial quantity of plagioclase phenocrysts that optically appear free of alteration (Fig. S4) for $^{40}Ar/^{39}Ar$ geochronology analysis.

$^{40}Ar/^{39}Ar$ analytical procedures

The samples were disaggregated by a SelFrag pulsed power fragmentation system at the John de Laeter Centre, Curtin University, and sieved to separate the 212–355 µm and 125–212 µm size fractions. These fractions were thoroughly rinsed in an ultrasonic cleaner to remove dust or powder from the grains. Minerals were separated using a Frantz isodynamic magnetic separator. Unaltered, optically transparent, inclusion-free plagioclase grains were handpicked carefully grain-by-grain under a binocular microscope from the non-magnetic fractions. Homogeneous groundmass grains were handpicked from the magnetic fractions. Grains showing evidence of alteration (e.g., brown, red, or yellow discoloration) were avoided where possible, but cryptic alteration was difficult to detect because groundmass is not transparent. The selected grains were leached in diluted (5 N) HF for 1 min and thoroughly rinsed in distilled water.

Multi-grain aliquots of the samples were loaded into several large wells, 1.9 cm diameter and 0.3 cm depth, within aluminium discs. A series of fully intercalibrated GA1550 biotite[66] standards with age 99.738 ± 0.100 Ma[67] were loaded adjacent to the samples in the same discs. The discs were Cd-shielded to minimize undesirable nuclear interference reactions and irradiated in the Oregon State University nuclear reactor (USA) in a central position for 40 h. For each disc, an average *J*-value was computed from standard grains within the small pits, and was used in the age calculations of samples (the unknowns) from pits surrounding those of the standards. The *J*-value for each sample is shown in Supplementary Data 1. Mass discrimination was monitored regularly through the analysis using an automated air pipette and mean values are 0.98754 ± 0.02, 0.99224 ± 0.05, and 0.99257 ± 0.02 (%1σ) per dalton (atomic mass unit) relative to an air ratio of 298.56 ± 0.31[68]. The correction factors for interfering isotopes were $(^{39}Ar/^{37}Ar)_{Ca} = 6.95 \times 10^{-4}$ (±1.3%), $(^{36}Ar/^{37}Ar)_{Ca} = 2.65 \times 10^{-4}$ (± 0.84%) and $(^{40}Ar/^{39}Ar)_{K} = 7.30 \times 10^{-4}$ (± 12%)[69]. The most important correction value required for Ca-rich samples (e.g., plagioclase) is $(^{36}Ar/^{37}Ar)_{Ca}$. This was re-measured and yielded a value of $(^{36}Ar/^{37}Ar)_{Ca} = 2.65 \times 10^{-4}$ (± 1.6%), in agreement with the value measured by Renne et al.[69]. The $^{40}Ar/^{39}Ar$ analyses were performed at the Western Australian Argon Isotope Facility at Curtin University. Multi-grain aliquots were step-heated using a continuous 100 W PhotonMachine© CO_2 (IR, 10.4 µm) laser fired on the samples for 60 s. Each of the standard crystals was fused in a single step.

The gas was purified in an extra low-volume stainless steel extraction line of 240 cc volume, using one SAES AP10 and one GP50 getter. The Ar isotopes were measured in static mode using a low volume (600 cc) Thermo Fisher Scientific ARGUS VI mass spectrometer set with a permanent resolution of ~200[70]. Measurements were performed in multi-collection mode using 4 Faraday cups with 10^{12} ohm resistors to measure masses of 40, 38, and 37 and a 10^{13} ohm resistor to measure mass 39. Mass 36 was measured using an ultralow background compact discrete dynode ion counter. We measured the relative abundance of each mass simultaneously using 10 cycles of peak-hopping and 16 s of integration time for each mass. Detectors were calibrated to each other electronically and using air shot beam signals.

The raw data were processed using the ArArCALC software[71] and the ages were calculated using the decay constants of Renne et al.[67]. Blanks were monitored every three to four steps. All parameters and relative abundance values are provided in Supplementary Data 1 following the recommendations of Schaen et al.[72], and corrected for blank, mass discrimination and radioactive decay. We consider a newly measured $^{40}Ar/^{39}Ar$ age robust only if it meets all the reliability criteria as detailed in the Supplementary Information. All the uncertainties of the $^{40}Ar/^{39}Ar$ ages are quoted at the 2σ confidence level.

Data availability

All data used in this manuscript are included in the Supplementary Information File and Supplementary Data 1 and 2.

References

1. Morgan, W. J. Convection plumes in the lower mantle. *Nature* **230**, 42–43 (1971).
2. Tarduno, J. A. et al. The Emperor Seamounts: Southward motion of the Hawaiian hotspot plume in Earth's mantle. *Science* **301**, 1064–1069 (2003).
3. Koppers, A. A. et al. Limited latitudinal mantle plume motion for the Louisville hotspot. *Nat. Geosci.* **5**, 911–917 (2012).
4. Steinberger, B., Sutherland, R. & O'Connell, R. J. Prediction of Emperor-Hawaii seamount locations from a revised model of global plate motion and mantle flow. *Nature* **430**, 167–173 (2004).
5. Torsvik, T. H. et al. Global plate motion frames: toward a unified model. *Rev. Geophys.* **46**, 2007RG000227 (2008).
6. Tarduno, J. A. & Koppers, A. A. When hot spots move: the new view of mantle dynamics made possible by scientific ocean drilling. *Oceanography* **32**, 150–152 (2019).
7. Steinberger, B. & O'Connell, R. J. Advection of plumes in mantle flow: implications for hotspot motion, mantle viscosity and plume distribution. *Geophys. J. Int.* **132**, 412–434 (1998).
8. Richards, M. A. & Griffiths, R. W. Deflection of plumes by mantle shear flow: experimental results and a simple theory. *Geophys. J. Int.* **94**, 367–376 (1988).

9. Griffiths, R. W. & Campbell, I. H. On the dynamics of long-lived plume conduits in the convecting mantle. *Earth Planet. Sci. Lett.* **103**, 214–227 (1991).
10. Tarduno, J., Bunge, H.-P., Sleep, N. & Hansen, U. The bent Hawaiian-Emperor hotspot track: inheriting the mantle wind. *Science* **324**, 50–53 (2009).
11. Sun, W. et al. Plume-ridge interaction induced migration of the Hawaiian-Emperor seamounts. *Sci. Bull.* **66**, 1691–1697 (2021).
12. Davaille, A., Girard, F. & Le Bars, M. How to anchor hotspots in a convecting mantle? *Earth Planet. Sci. Lett.* **203**, 621–634 (2002).
13. Bono, R. K., Tarduno, J. A. & Bunge, H.-P. Hotspot motion caused the Hawaiian-Emperor Bend and LLSVPs are not fixed. *Nat. Commun.* **10**, 3370 (2019).
14. Hassan, R. et al. A rapid burst in hotspot motion through the interaction of tectonics and deep mantle flow. *Nature* **533**, 239–242 (2016).
15. French, S. W. & Romanowicz, B. Broad plumes rooted at the base of the Earth's mantle beneath major hotspots. *Nature* **525**, 95–99 (2015).
16. Dongmo Wamba, M., Montagner, J.-P. & Romanowicz, B. Imaging deep-mantle plumbing beneath La Réunion and Comores hot spots: vertical plume conduits and horizontal ponding zones. *Sci. Adv.* **9**, eade3723 (2023).
17. Davaille, A. & Romanowicz, B. Deflating the LLSVPs: bundles of mantle thermochemical plumes rather than thick stagnant "piles". *Tectonics* **39**, e2020TC006265 (2020).
18. Tsekhmistrenko, M., Sigloch, K., Hosseini, K. & Barruol, G. A tree of Indo-African mantle plumes imaged by seismic tomography. *Nat. Geosci.* **14**, 612–619 (2021).
19. Sager, W. W. Is "plume interaction induced migration of the Hawaiian-Emperor Seamounts" a step too far? *Sci. Bull.* **67**, 1217–1220 (2022).
20. Konrad, K. et al. On the relative motions of long-lived Pacific mantle plumes. *Nat. Commun.* **9**, 854 (2018).
21. Weis, D., Frey, F. A., Giret, A. & Cantagrel, J.-M. Geochemical characteristics of the youngest volcano (Mount Ross) in the Kerguelen Archipelago: inferences for magma flux, lithosphere assimilation and composition of the Kerguelen plume. *J. Petrol.* **39**, 973–994 (1998).
22. Fox, J. M. et al. Construction of an intraplate island volcano: the volcanic history of Heard Island. *Bull. Volcanol.* **83**, 37 (2021).
23. Duncan, R. A., Quilty, P. G., Barling, J. & Fox, J. M. Geological development of Heard Island, Central Kerguelen Plateau. *Aust. J. Earth Sci.* **63**, 81–89 (2016).
24. Jiang, Q. et al. Longest continuously erupting large igneous province driven by plume-ridge interaction. *Geology* **49**, 206–210 (2021).
25. Coffin, M. F. et al. Kerguelen hotspot magma output since 130 Ma. *J. Petrol.* **43**, 1121–1139 (2002).
26. Zhang, Z. et al. The evolution of Kerguelen mantle plume and breakup of eastern Gondwana: new insights from multistage Cretaceous magmatism in the Tethyan Himalaya. *Gondwana Res.* **119**, 68–85 (2023).
27. Duncan, R. A. Age distribution of volcanism along aseismic ridges in the eastern Indian Ocean. In: *Proceedings of the Ocean Drilling Program, Scientific Results*) (1991).
28. Krishna, K. S. et al. Tectonics of the Ninetyeast Ridge derived from spreading records in adjacent oceanic basins and age constraints of the ridge. *J. Geophys. Res. Solid Earth* **117**, B04101 (2012).
29. Royer, J. Tectonic constraints on the hotspot formation of Ninetyeast Ridge. *Proc. Ocean Drill. Program Sci. Results* **121**, 763–776 (1991).
30. Steinberger, B. & O'Connell, R. J. Effects of mantle flow on hotspot motion. *Hist. Dyn. Glob. Plate Motions* **121**, 377–398 (2000).
31. O'Neill, C., Müller, D. & Steinberger, B. On the uncertainties in hot spot reconstructions and the significance of moving hot spot reference frames. *Geochem. Geophys. Geosyst.* **6**, Q04003 (2005).
32. O'Neill, C., Müller, D. & Steinberger, B. Geodynamic implications of moving Indian Ocean hotspots. *Earth Planet. Sci. Lett.* **215**, 151–168 (2003).
33. Steinberger, B. & Antretter, M. Conduit diameter and buoyant rising speed of mantle plumes: implications for the motion of hot spots and shape of plume conduits. *Geochem. Geophys. Geosyst.* **7**, Q11018 (2006).
34. Klootwijk, C. T., Gee, J. S., Peirce, J. W. & Smith, G. M. Constraints on the India–Asia convergence: paleomagnetic results from Ninetyeast ridge. *Proc. Ocean Drill. Program Sci. Results* **121**, 777–882 (1991).
35. Antretter, M., Steinberger, B., Heider, F. & Soffel, H. Paleolatitudes of the Kerguelen hotspot: new paleomagnetic results and dynamic modeling. *Earth Planet. Sci. Lett.* **203**, 635–650 (2002).
36. Peirce, J. W. The northward motion of India since the Late Cretaceous. *Geophys. J. Int.* **52**, 277–311 (1978).
37. Sharp, W. D. & Renne, P. R. The $^{40}Ar/^{39}Ar$ dating of core recovered by the Hawaii Scientific Drilling Project (phase 2), Hilo, Hawaii. *Geochem. Geophys. Geosyst.* **6**, Q04G17 (2005).
38. Tarduno, J. A. On the motion of Hawaii and other mantle plumes. *Chem. Geol.* **241**, 234–247 (2007).
39. Koppers, A. A., Duncan, R. A. & Steinberger, B. Implications of a nonlinear $^{40}Ar/^{39}Ar$ age progression along the Louisville seamount trail for models of fixed and moving hot spots. *Geochem. Geophys. Geosyst.* **5**, Q06L02 (2004).
40. Duncan, R. Geochronology of basalts from the Ninetyeast Ridge and continental dispersion in the eastern Indian Ocean. *J. Volcanol. Geotherm. Res.* **4**, 283–305 (1978).
41. Jiang, Q. et al. $^{40}Ar/^{39}Ar$ dating of basaltic rocks and the pitfalls of plagioclase alteration. *Geochim. Cosmochim. Acta* **314**, 334–357 (2021).
42. Davidson, P. C., Koppers, A. A., Sano, T. & Hanyu, T. A younger and protracted emplacement of the Ontong Java Plateau. *Science* **380**, 1185–1188 (2023).
43. Jiang, Q., & Jourdan, F. Obtaining accurate ages of basaltic rocks using $^{40}Ar/^{39}Ar$ techniques. In: *Methods and Applications of Geochronology* (eds Shellnutt J. G., Denyszyn S. W., Suga K.). Elsevier (2024).
44. Pringle, M., Frey, F., Mervine, E., & Sager, W. New Ar/Ar ages from the Ninetyeast Ridge, Indian Ocean: beginning of a robust Indo-Atlantic hotspot reference frame. In: *AGUFM*) (2007).
45. Pringle, M., Frey, F., & Mervine, E. A simple linear age progression for the Ninetyeast Ridge, Indian Ocean: new constraints on Indian plate tectonics and hotspot dynamics. In: *AGUFM*) (2008).
46. Pringle, M., Frey, F., & Meleney, P. Ninetyeast Ridge formed as a single, near spreading center, hotspot track. In: *AGUFM*) (2011).
47. Gibbons, A. D., Whittaker, J. M. & Müller, R. D. The breakup of East Gondwana: assimilating constraints from Cretaceous ocean basins around India into a best-fit tectonic model. *J. Geophys. Res. Solid Earth* **118**, 808–822 (2013).
48. Van Hinsbergen, D. J. et al. Greater India Basin hypothesis and a two-stage Cenozoic collision between India and Asia. *Proc. Natl Acad. Sci. USA* **109**, 7659–7664 (2012).
49. Cande, S. C. & Stegman, D. R. Indian and African plate motions driven by the push force of the Reunion plume head. *Nature* **475**, 47–52 (2011).
50. Seton, M. et al. Global continental and ocean basin reconstructions since 200. *Ma. Earth-Sci. Rev.* **113**, 212–270 (2012).
51. Jagoutz, O., Royden, L., Holt, A. F. & Becker, T. W. Anomalously fast convergence of India and Eurasia caused by double subduction. *Nat. Geosci.* **8**, 475–478 (2015).
52. Steinberger, B. & Torsvik, T. H. A geodynamic model of plumes from the margins of Large Low Shear Velocity Provinces. *Geochem. Geophys. Geosyst.* **13**, Q01W09 (2012).
53. Weis, D., Frey, F. A. Isotope geochemistry of Ninetyeast Ridge basement basalts: Sr, Nd, and Pb evidence for involvement of the

Kerguelen hot spot. In: *Proceedings of the Ocean Drilling Program, Scientific Results*) (1991).
54. Nobre Silva, I. G., Weis, D., Scoates, J. S. & Barling, J. The Ninetyeast Ridge and its relation to the Kerguelen, Amsterdam and St. Paul hotspots in the Indian Ocean. *J. Petrol.* **54**, 1177–1210 (2013).
55. Frey, F. et al. Diverse mantle sources for Ninetyeast Ridge magmatism: geochemical constraints from basaltic glasses. *Earth Planet. Sci. Lett.* **303**, 215–224 (2011).
56. Frey, F. A. et al. Depleted components in the source of hotspot magmas: evidence from the Ninetyeast Ridge (Kerguelen). *Earth Planet. Sci. Lett.* **426**, 293–304 (2015).
57. Weis, D., Frey, F., Leyrit, H. & Gautier, I. Kerguelen Archipelago revisited: geochemical and isotopic study of the Southeast Province lavas. *Earth Planet. Sci. Lett.* **118**, 101–119 (1993).
58. Doucet, S. et al. The depleted mantle component in Kerguelen Archipelago basalts: petrogenesis of tholeiitic–transitional basalts from the Loranchet Peninsula. *J. Petrol.* **43**, 1341–1366 (2002).
59. Duncan, R. A. A time frame for construction of the Kerguelen Plateau and Broken Ridge. *J. Petrol.* **43**, 1109–1119 (2002).
60. Duncan, R. A., Falloon, T. J., Quilty, P. G. & Coffin, M. F. Widespread Neogene volcanism on Central Kerguelen Plateau, Southern Indian Ocean. *Aust. J. Earth Sci.* **63**, 379–392 (2016).
61. Weis, D. et al. Trace of the Kerguelen mantle plume: evidence from seamounts between the Kerguelen Archipelago and Heard Island, Indian Ocean. *Geochem. Geophys. Geosyst.* **3**, 1–27 (2002).
62. Vandamme, D., Courtillot, V. Paleomagnetism of Leg 115 basement rocks and latitudinal evolution of the Reunion hotspot. In: *Proc. ODP Sci. Results*. (1990).
63. Torsvik, T. et al. Late cretaceous magmatism in Madagascar: palaeomagnetic evidence for a stationary Marion hotspot. *Earth Planet. Sci. Lett.* **164**, 221–232 (1998).
64. Celli, N. L., Lebedev, S., Schaeffer, A. J. & Gaina, C. The tilted Iceland Plume and its effect on the North Atlantic evolution and magmatism. *Earth Planet. Sci. Lett.* **569**, 117048 (2021).
65. Barruol, G. et al. Large-scale flow of Indian Ocean asthenosphere driven by Réunion plume. *Nat. Geosci.* **12**, 1043–1049 (2019).
66. Renne, P. R. et al. Intercalibration of standards, absolute ages and uncertainties in $^{40}Ar/^{39}Ar$ dating. *Chem. Geol.* **145**, 117–152 (1998).
67. Renne, P. R. et al. Response to the comment by W.H. Schwarz et al. on "Joint determination of ^{40}K decay constants and $^{40}Ar^*/^{40}K$ for the Fish Canyon sanidine standard, and improved accuracy for $^{40}Ar/^{39}Ar$ geochronology" by P.R. Renne et al. (2010). *Geochim. Cosmochim. Acta* **75**, 5097–5100 (2011).
68. Lee, J. Y. et al. A redetermination of the isotopic abundances of atmospheric Ar. *Geochim. Cosmochim. Acta* **70**, 4507–4512 (2006).
69. Renne, P. R. et al. Time scales of critical events around the Cretaceous-Paleogene boundary. *Science* **339**, 684–687 (2013).
70. Jourdan, F. et al. Collisional history of asteroid Itokawa. *Geology* **45**, 819–822 (2017).
71. Koppers, A. A. P. ArArCALC—software for $^{40}Ar/^{39}Ar$ age calculations. *Comput. Geosci.* **28**, 605–619 (2002).
72. Schaen, A. J. et al. Interpreting and reporting $^{40}Ar/^{39}Ar$ geochronologic data. *Geol. Soc. Am. Bull.* **133**, 461–487 (2021).
73. Ryan, W. B. F. et al. Global multi-resolution topography synthesis. *Geochem. Geophys. Geosyst.* **10**, Q03014 (2009).
74. Cande, S. C., Patriat, P. & Dyment, J. Motion between the Indian, Antarctic and African plates in the early Cenozoic. *Geophys. J. Int.* **183**, 127–149 (2010).
75. Copley, A., Avouac, J. P. & Royer, J. Y. India-Asia collision and the Cenozoic slowdown of the Indian plate: Implications for the forces driving plate motions. *J. Geophys. Res. Solid Earth* **115**, B03410 (2010).

Acknowledgements

This research was financially supported by the Australian Antarctic Division Science Project (#4446). We are grateful to Ellen Roosen at the Woods Hole Oceanographic Institution (USA), and Yusuke Kubo and the team at the Kochi Core Center (Japan) for the ease of sample acquisitions. Celia Mayers and Adam Frew at the Western Australian Argon Isotope Facility are thanked for their help in sample preparation and $^{40}Ar/^{39}Ar$ geochronology analysis. Q.J. acknowledges support from the National Natural Science Foundation of China (#42302339) and the Fundamental Research Funds for the Central Universities (#2462022BJRC011).

Author contributions

Q.J. obtained the drilling hole samples, analysed and interpreted the data, and wrote the original manuscript. H.K.H.O. obtained the dredge samples and funding, and analysed the data. F.J. obtained funding, conducted the geochronological analyses, and analysed the data. D.C.H. prepared the drilling hole samples for geochronological analyses. R.E.M. obtained funding and analysed the data. E.M.M. and W.W.S. supplied the dredge samples. All authors contributed to the editing of the manuscript.

Competing interests

The authors declare no competing interests.

Additional information

Supplementary information The online version contains supplementary material available at https://doi.org/10.1038/s41467-024-54092-6.

Correspondence and requests for materials should be addressed to Qiang Jiang.

Peer review information *Nature Communications* thanks Bernhard Steinberger and the other, anonymous, reviewer(s) for their contribution to the peer review of this work. A peer review file is available.